Original Article

MOLECULAR METABOLISM

White matter fiber-specific degeneration in older adults with metabolic syndrome

Christina Andica [1,2,*], Koji Kamagata [2], Wataru Uchida [2], Kaito Takabayashi [2], Keigo Shimoji [2], Hideyoshi Kaga [3,4], Yuki Someya [3], Yoshifumi Tamura [3,4], Ryuzo Kawamori [3,4], Hirotaka Watada [3,4], Masaaki Hori [2,5], Shigeki Aoki [2]

ABSTRACT

Objective: Metabolic syndrome (MetS) is defined as a complex of interrelated risk factors for type 2 diabetes and cardiovascular disease, including glucose intolerance, abdominal obesity, hypertension, and dyslipidemia. Studies using diffusion tensor imaging (DTI) have reported white matter (WM) microstructural abnormalities in MetS. However, interpretation of DTI metrics is limited primarily due to the challenges of modeling complex WM structures. The present study used fixel-based analysis (FBA) to assess the effect of MetS on the fiber tract-specific WM microstructure in older adults and its relationship with MetS-related measurements and cognitive and locomotor functions to better understand the pathophysiology of MetS.

Methods: Fixel-based metrics, including microstructural fiber density (FD), macrostructural fiber-bundle cross-section (FC), and a combination of FD and FC (FDC), were evaluated in 16 healthy controls (no components of MetS; four men; mean age, 71.31 $\pm$ 5.06 years), 57 individuals with premetabolic syndrome (preMetS; one or two components of MetS; 29 men; mean age, 72.44 $\pm$ 5.82 years), and 46 individuals with MetS (three to five components of MetS; 27 men; mean age, 72.15 $\pm$ 4.97 years) using whole-brain exploratory FBA. Tract of interest (TOI) analysis was then performed using TractSeg across 14 selected WM tracts previously associated with MetS. The associations between fixel-based metrics and MetS-related measurements, neuropsychological, and locomotor function tests were also analyzed in individuals with preMetS and MetS combined. In addition, tensor-based metrics (i.e., fractional anisotropy [FA] and mean diffusivity [MD]) were compared among the groups using tract-based spatial statistics (TBSS) analysis.

Results: In whole-brain FBA, individuals with MetS showed significantly lower FD, FC, and FDC compared with healthy controls in WM areas, such as the splenium of the corpus callosum (CC), corticospinal tract (CST), middle cerebellar peduncle (MCP), and superior cerebellar peduncle (SCP). Meanwhile, in fixel-based TOI, significantly reduced FD was observed in individuals with preMetS and MetS in the anterior thalamic radiation, CST, SCP, and splenium of the CC compared with healthy controls, with relatively greater effect sizes observed in individuals with MetS. Compared with healthy controls, significantly reduced FC and FDC were only demonstrated in individuals with MetS, including regions with loss of FD, inferior cerebellar peduncle, inferior fronto-occipital fasciculus, MCP, and superior longitudinal fasciculus part I. Furthermore, negative correlations were observed between FD and Brinkman index of cigarette consumption cumulative amount and between FC or FDC and the Trail Making Test (parts B—A), which is a measure of executive function, waist circumference, or low-density lipoprotein cholesterol. Finally, TBSS analysis revealed that FA and MD were not significantly different among all groups.

Conclusions: The FBA results demonstrate that substantial axonal loss and atrophy in individuals with MetS and early axonal loss without fiber-bundle morphological changes in those with preMetS within the WM tracts are crucial to cognitive and motor function. FBA also clarified the association between executive dysfunction, abdominal obesity, hyper-low-density lipoprotein cholesterolemia, smoking habit, and compromised WM neural tissue microstructure in MetS.

Keywords Diffusion MRI; Executive-motor dysfunction; Fixel-based analysis; Metabolic syndrome; Neurodegeneration; White matter

1. INTRODUCTION

Metabolic syndrome (MetS) is a complex of interrelated risk factors for type 2 diabetes and cardiovascular disease, including glucose intolerance, abdominal obesity, hypertension, and dyslipidemia, that is associated with increased mortality and morbidity rates [1]. It is a common public health and major clinical problem due to its continuing growth in prevalence worldwide [1]. The effects of MetS are multiple and wide-ranging. Recent studies have suggested the presence of widespread white matter (WM) microstructural abnormalities in

[1]Faculty of Health Data Science, Juntendo University, Urayasu, Chiba, 279-0013, Japan [2]Department of Radiology, Juntendo University Graduate School of Medicine, Bunkyo, Tokyo, 113-8421, Japan [3]Sportology Center, Juntendo University Graduate School of Medicine, Bunkyo, Tokyo, 113-0034, Japan [4]Department of Metabolism & Endocrinology, Juntendo University Graduate School of Medicine, Bunkyo, Tokyo, 113-8421, Japan [5]Department of Radiology, Toho University Omori Medical Center, Ota, Tokyo, 143-8541, Japan

*Corresponding author. Faculty of Health Data Science, Juntendo University, 6-8-1 Hinode, Urayasu, Chiba, 279-0013, Japan. E-mail: christina@juntendo.ac.jp (C. Andica).

Received April 28, 2022 • Revision received June 5, 2022 • Accepted June 6, 2022 • Available online 9 June 2022

https://doi.org/10.1016/j.molmet.2022.101527

Abbreviations

AF	arcuate fasciculus
ATR	anterior thalamic radiation
CC	corpus callosum
CSD	constrained spherical deconvolution
CST	corticospinal tract
DTI	diffusion tensor imaging
FA	fractional anisotropy
FBA	fixel-based analysis
FC	fiber-bundle cross-section
FD	fiber density
FDC	fiber density and cross-section
FDR	false discovery rate
FODs	fiber orientation distributions
FWE	family-wise error
GDS-15-J	Japanese version of the 15-item Geriatric Depression Scale
HDL	high-density lipoprotein
HOMA-IR	homeostasis model assessment of insulin
ICP	inferior cerebellar peduncle
ICV	intracranial volume
IFO	inferior fronto-occipital fasciculus
ILF	inferior longitudinal fasciculus
LDL	low-density lipoprotein
MCP	middle cerebellar peduncle
MD	mean diffusivity
MetS	metabolic syndrome
preMetS	premetabolic syndrome
SCP	superior cerebellar peduncle
SLF	superior longitudinal fasciculus
TBSS	tract-based spatial statistics
TMT	trail making test
TOI	tract of interest
UF	uncinate fasciculus
WM	white matter

individuals with MetS, which lead to cognitive impairment and increased risk of dementia later in life [2]. In addition to cognitive dysfunctions, a poorer locomotor function has recently been observed in individuals with MetS [3]. Despite a clear connection, the pathological mechanisms underlying cognitive and locomotor impairments in MetS are not fully understood yet.

Diffusion tensor imaging (DTI) is the current most widely used tool used to assess WM microstructural alterations. However, it is limited by its inability to represent the diffusion signal in crossing or kissing fiber regions. It has been suggested that approximately 90% of WM voxels at the current limit of resolution of diffusion-weighted imaging (2.4 mm isotropic voxel size) contain multiple fiber populations [4]. Furthermore, the tensor model has been shown to lack specificity regarding pathology [5]. Lower fractional anisotropy (FA) and/or higher mean diffusivity (MD) have been observed in the WM of individuals with MetS [6,7], indicating alterations in axonal diameter/density and/or myelin content [5]. Taken together, these limitations lead to an unreliable interpretation of DTI-associated metrics.

Fixel-based analysis (FBA) was proposed to quantify the properties of WM fiber in its complex fiber geometry. The term "fixel" refers to a specific individual fiber population within a voxel [8,9] and is derived from WM fiber orientation distributions (FODs) as computed by constrained spherical deconvolution (CSD) method [10]. FBA enables the measurement of microstructural differences in fiber density (FD), macrostructural differences in the fiber-bundle cross-section (FC), or differences arising from the combination of FD and FC (fiber density and cross-section [FDC]) [9]. Adoption of the FBA framework has increased over the years, as summarized by Dhollander et al. [11]. For example, studies using FBA in healthy adults reported widespread age-related decreases in FD, FC, and FDC indicative of WM degradation with age [12,13]. Changes in fixel-based metrics have also been observed in neurodegenerative diseases, such as Alzheimer's disease [14] and Parkinson's disease [15–18].

The present study used FBA to assess the effect of MetS on the WM fiber-specific microstructure in older adults and its relationship with MetS-related measurements and cognitive and locomotor functions to better understand the pathophysiology of MetS. Time-course gene expression profiles of a mouse model of MetS revealed a predisease state prior to MetS [19]. Therefore, we evaluated individuals with components of MetS who did not meet the criteria for diagnosis of MetS or premetabolic syndrome (preMetS) to determine the early signs of fiber tract-specific degeneration, which is considered the optimal time for preventive treatment [19]. Finally, we assessed DTI metrics for comparison.

2. PARTICIPANTS AND METHODS

2.1. Metabolic syndrome criteria

We defined MetS according to the guidelines of the International Diabetes Federation and the American Heart Association/National Heart, Lung, and Blood Institute [1]—which have been reported to be the most suitable for clinical practice and are ethnically specific [20]—as the presence of at least three of the following five risk factors: (1) abdominal obesity (waist circumference $\geq$85 cm for men and $\geq$90 cm for women, adjusted for Japanese individuals [21]); (2) elevated blood pressure (systolic pressure $\geq$130 mmHg and/or diastolic pressure $\geq$85 mmHg or receiving treatment for hypertension); (3) elevated fasting plasma glucose levels ($\geq$100 mg/dL or receiving treatment for hyperglycemia); (4) elevated triglyceride levels ($\geq$150 mg/dL or receiving treatment for hypertriglyceridemia); and (5) low levels of high-density lipoprotein (HDL) cholesterol ($<$40 mg/dL or receiving treatment). Individuals with no risk factors were categorized as healthy controls, whereas those with one or two risk factors were categorized as preMetS [22].

2.2. Study participants

Data for the study participants were obtained from the Bunkyo Health Study [23], which was a prospective cohort study of older individuals (age, 65–84 years) in an urban community. The study protocol was approved by the ethics committee of Juntendo University, and all individuals provided written informed consent prior to participating in the study.

Inclusion criteria were as follows: available and complete data for MetS-related characteristics, neuropsychological measures, locomotor function tests, assessment of WM hyperintensities (Fazekas scale), and brain 3T magnetic resonance imaging (MRI) results. Exclusion criteria were as follows: history of drug and/or alcohol abuse; past or present neurological or psychiatric disorders; dementia (mini-mental state examination [MMSE] score of $\leq$23) [24], depression (the Japanese version of the 15-item Geriatric Depression scale [GDS-15-J] score of $\geq$10) [25]; or structural brain MRI abnormalities.

2.3. Metabolic syndrome-related assessments

Among Japanese individuals, the cutoff values for waist circumference used in this study were based on the cutoff values of visceral fat area determined using computed tomography (CT) scan [26]. Visceral fat deposition at the navel level of >100 cm^2, corresponding to a waist circumference of 85 or 90 cm for Japanese males or females, respectively, is associated with higher prevalence of MetS risk factors. The cutoff value is larger for females because the amount of subcutaneous fat is greater in women than in men when visceral adiposity is equivalent, although there is substantial variation between individuals. The areas of visceral and subcutaneous fat were measured using a 0.3 T MRI scanner after overnight fasting as described previously by Someya et al. [23]. Notably, the MRI measurements were in good agreement with the CT findings, which is considered the gold standard [27]. Arteriosclerosis was predicted using the cardio-ankle vascular index (CAVI), which is an index of overall arterial stiffness and is independent of blood pressure [28]. Insulin resistance was assessed using the homeostasis model assessment of insulin resistance (HOMA-IR) based on the fasting glucose and insulin plasma levels [29].

2.4. Neuropsychological tests

The present study evaluated global cognitive function, as measured by the Japanese version of the Montreal Cognitive Assessment (MOCA-J) [30] and MMSE [24], and the difference between time (in seconds) spent in completing parts B and A of the trail-making test (TMT [B−A]) to measure cognitive flexibility and executive function [31].

2.5. Locomotor function tests

The term "locomotive syndrome" was proposed by the Japanese Orthopaedic Association in 2007 to describe a condition of reduced mobility (sit-to-stand or gait) due to age-related impairment of the locomotor system, which includes the bone, cartilage, muscle, and nervous system [32]. The risk of locomotive syndrome is measured using the stand-up test, two-step test, and 25-question geriatric locomotive function scale (GLFS-25). Detailed descriptions of these tests are available in previous studies [33,34]. The two-step test score (length of two steps in cm) is standardized using the individual's height (cm). The study participants were classified as no locomotive syndrome (stage 0), locomotive syndrome stage 1, or locomotive syndrome stage 2. Locomotive syndrome stage 1 (beginning to decline in mobility) is defined as a two-step test score of <1.3 and difficulty with one-leg standing from a 40-cm seat in the stand-up test (either leg), or a GLFS-25 score of ≥ 7 [33]. Locomotive syndrome stage 2 (progressing to a decline in mobility) was defined as a two-step test score of <1.1 and difficulty standing from a 20-cm seat using both legs in the stand test or a GLFS-25 score of ≥ 16 [33].

2.6. Imaging protocols

All imaging data were acquired using the 3 T system (MAGNETOM Prisma; Siemens Healthcare, Erlangen, Germany) with a 64-channel head coil. Three-dimensional T1-weighted images were obtained using a magnetization-prepared rapid gradient echo protocol (echo time [TE], 2.32 ms; repetition time [TR], 2300 ms; inversion time, 900 ms; field of view [FOV], 240 mm $\times$ 240 mm; matrix size, 256 $\times$ 256; slice thickness, 0.9 mm; and acquisition time, 5.21 min). Diffusion-weighted images were obtained using echo planar imaging in the anterior−posterior phase-encoding direction with the following parameters: TE, 70 ms; TR, 3300 ms; FOV, 229 mm $\times$ 229 mm; matrix size, 130 $\times$ 130; slice thickness, 1.8 mm; *b*-values, 1000 and 2000 s/mm^2; 64 isotropic gradient directions; one non-diffusion-weighted ($b = 0$) volume; and acquisition time, 7.29 min. The standard and reverse phase-encoded blipped images with no diffusion weighting (blip up and blip down) were also obtained to correct for magnetic susceptibility-induced distortions related to echo-planar imaging acquisition [35].

2.7. Fixel-based analysis pipeline

FBA was performed according to the recommended pipeline [9,11]. Preprocessing steps of diffusion-weighted images—including denoising [36], removal of Gibbs ringing artifacts, eddy-current and motion-induced distortion correction [37], bias field correction [38], and up-sampling diffusion-weighted image spatial resolution to an isotropic voxel size of 1 mm [39]—were performed using MRtrix3 (http://mrtrix.org). We estimated FODs for each participant using the multishell multitissue-CSD algorithm with the group-average response functions of WM, gray matter, and cerebrospinal fluid [10]. The remaining processing steps included overall image intensity normalization of FOD images to enable the comparison of FOD amplitudes among participants using the median b $= 0$ intensity and the generation of a study-specific FOD template using FOD images from all participants with linear and nonlinear registration [39,40]. The study-specific population template was then transformed into MNI152 common space using FA-based affine registration in the FMRIB Software Library 5.0.9 (FSL; Oxford Centre for Functional MRI of the Brain, UK; www.fmrib.ox.ac.uk/fsl).

The following fixel-based metrics were calculated (Figure 1): (1) FD, which measures the intra-axonal volume of axons of a fiber population in each voxel compartment [9,11]. (2) FC, which is a morphological measure of fiber-bundle cross-sectional size that is calculated as the extent of distortion in a bundle cross-section required to warp a participant's FOD into the template image [9,11]. Before statistical analysis, FC was log-transformed (log-FC) to ensure zero-centered and normally distributed data. (3) FDC, which is a combined measure of FD and FC (multiplicative) that accounts for both microscopic and macroscopic changes in a fiber bundle, thereby providing sensitivity to any differences related to the capacity of the WM to transmit information [9,11].

2.8. Tract of interest analysis

Tract of interest (TOI) analysis was performed to investigate further potential WM degeneration of fiber pathways in individuals with pre-MetS and MetS. WM tract segmentation was conducted using the TractSeg algorithm [41]. TractSeg was applied to the study-specific population template, which had been transformed into MNI152 common space [42]. We delineated WM tracts (Figure 2) previously implicated in MetS or individual components of MetS including arcuate fasciculus (AF), anterior thalamic radiation (ATR), cingulum, corticospinal tract (CST), inferior cerebellar peduncle (ICP), inferior fronto-occipital fasciculus (IFO), inferior longitudinal fasciculus (ILF), middle cerebellar peduncle (MCP), superior cerebellar peduncle (SCP), splenium of the corpus callosum (CC), superior longitudinal fasciculus (SLF)-I, SLF-II, and SLF-III, and uncinate fasciculus (UF) [2]. The anatomical definition and functions of the WM regions are described in Supplementary Table 1. The FD, log-FC, and FDC maps from each participant were then cropped to only include fixels belonging to the tracts of interest, leaving 14 (splenium of the CC and bilateral AF, ATR, cingulum, CST, ICP, IFO, ILF, MCP, SCP, SLF-I, SLF-II, SLF-III, and UF) fixel maps for each fixel-based metric. These fixel maps were then statistically analyzed.

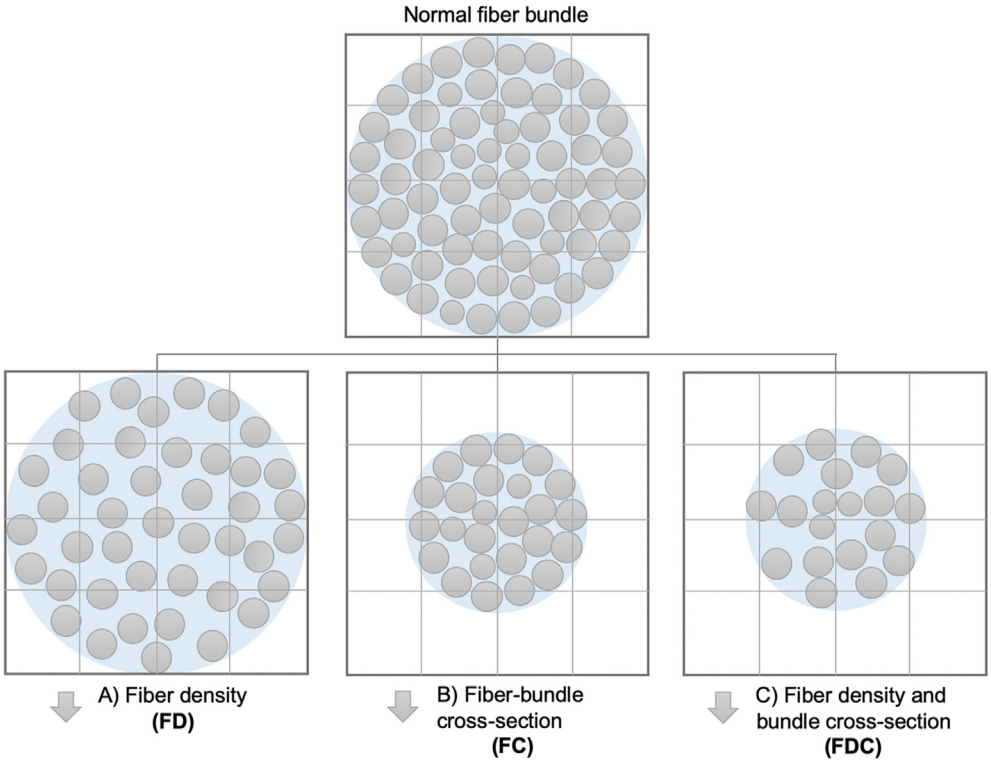

Figure 1: Fixel-based metrics. Schematic represents a fiber-bundle cross-section (light blue) containing numerous axons (gray circles) in imaging voxels (grid). Changes to the intra-axonal volume may manifest as: (A) differences in the tissue microstructure that result in changes to the within-voxel fiber density (axonal loss); (B) macroscopic differences in the fiber-bundle cross-section (fiber-bundle atrophy); or (C) differences in both the fiber density and bundle cross-section (axonal loss and atrophy).

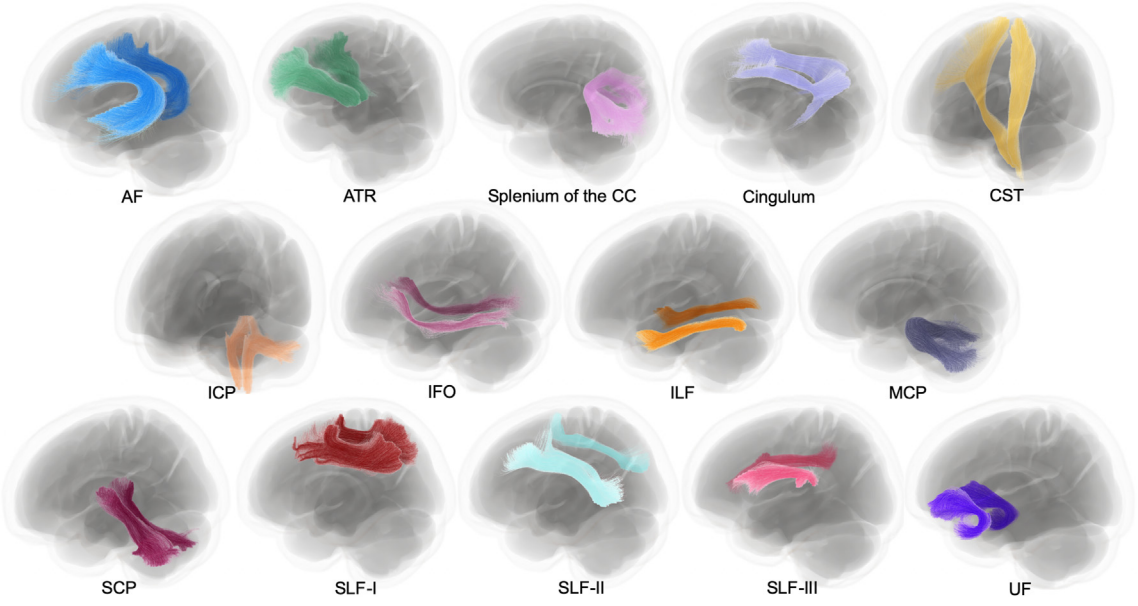

Figure 2: White matter tracts of interest. White matter pathways reconstructed using TractSeg and visualized in MRtrix3. The shown tracts are explanatory at the group level and were derived by applying TractSeg to the study-specific population template in MNI152 common space. AF, arcuate fasciculus; ATR, anterior thalamic radiation; CC, corpus callosum; CST, corticospinal tract; ICP, inferior cerebellar peduncle; IFO, inferior fronto-occipital fasciculus; ILF, inferior longitudinal fasciculus; MCP, middle cerebellar peduncle; SCP, superior cerebellar peduncle; SLF, superior longitudinal fasciculus; UF, uncinate fasciculus.

2.9. Tensor-derived metrics

The DTIFIT tool, which is a part of the FSL, was used to generate FA and MD maps for each participant using preprocessed diffusion-weighted data with *b*-values of 0 and 1000 s/mm^2. Between-group comparisons of FA and MD were performed using tract-based spatial statistics (TBSS) [43], which is currently the most commonly used voxel-wise

statistical analysis of WM diffusion-weighted imaging data [43]. The TBSS procedure was as follows: (1) FA maps of all participants were aligned in $1 \times 1 \times 1$ mm^3 MNI152 common space (an averaged brain) using the nonlinear registration tool in the FMRIB Software Library 5.0.9 (Oxford Centre for Functional MRI of the Brain, UK; www.fmrib.ox.ac.uk/fsl) [44]. (2) a population-based mean FA image was created and thinned to generate a mean FA skeleton representing the centers of all tracts common to the group. The threshold FA level of this skeleton was 0.2 to exclude voxels from gray matter and cerebrospinal fluid. (3) The averaged FA map for each participant was projected onto the skeleton. Finally, the mean diffusivity maps were projected onto the FA-derived skeleton after applying each participant's warping registration to the common space.

2.10. Intracranial volume measurements

The estimated intracranial volume (ICV) was obtained for each study participant using T1-weighted images in FreeSurfer version 6.0.0 (http://surfer.nmr.mgh.harvard.edu/fswiki) with the recon-all pipeline [45]. The ICV was used as a nuisance covariate in statistical analyses.

2.11. Statistical analysis

Kolmogorov–Smirnov test was used to assess the normality of the data in IBM SPSS Statistics version 27.0 (IBM Corporation, Armonk, NY, USA). Demographic and clinical data were analyzed using one-way analysis of variance with Tukey's honest significant difference post hoc test or Kruskal–Wallis with Mann–Whitney U post hoc test for normally or nonnormally distributed continuous data, respectively, whereas chi-square test was used for categorical variables. *P*-values (two-tailed) of <0.05 were considered statistically significant.

For each fixel-wise metric, a connectivity-based fixel enhancement for statistical inference [8] with default smoothing parameters (smoothing, 10 mm full-width at half maximum; C, 0.5; E, 2, and H, 3) was performed in whole-brain (including 2 million streamlines from the template tractogram) and TOI analyses. A general linear model framework was applied to compare: (1) healthy controls vs. preMetS; (2) healthy controls vs. MetS; and (3) preMetS vs. MetS. Age, sex, and years of education were included as nuisance covariates. Log-transformed ICV (log-ICV) was included as a nuisance covariate for log-FC and FDC (but not FD) to avoid false-positive results with global effects of brain scaling resulting from the registration to a template removed [9,46]. Family-wise error (FWE)-corrected *P*-values were then assigned to each fixel using nonparametric permutation testing with 10,000 permutations. FWE-corrected *P*-values <0.05 were considered statistically significant for whole-brain FBA. Statistical analyses were conducted separately for each tract in the TOI analysis; thus, FWE-corrected *P*-value at the peak fixel level within each tract were then submitted for false discovery rate (FDR) correction for multiple comparisons across 14 WM tracts. Tracts with peak pixel FWE-corrected *P*-values <0.05 following FDR correction were considered to withstand correction for multiple comparisons across tracts. Significant fixels in both whole-brain and TOI statistical analyses were displayed using the *mrview* tool in MRtrix3. Streamlines from template-derived tractogram were cropped to include only fixels that were significant (FWE-corrected $P < 0.05$) and color-coded by the effect size expressed as a percentage relative to the control group.

We also assessed the associations between mean values of fixel-based metrics along each tested WM tract (Supplementary Table 2) and the MetS-related measurements, neuropsychological tests, locomotor function tests (Table 1) in individuals with preMetS and MetS combined using partial correlation tests adjusting for age, sex, and years of education in SPSS 27. FDR-adjusted (for 14 WM tracts) *P*-values of <0.05 (two-tailed) were considered significant.

For TBSS analysis, a voxel-wise general linear model framework, including age, sex, years of education, and log-ICV as covariates, was used to compare FA and MD between all groups using the FSL randomize tool with 10,000 permutations. Between-group differences were considered significant at $P < 0.05$ and corrected for multiple comparisons using the FWE and threshold-free cluster enhancement approaches.

3. RESULTS

3.1. Demographic and clinical assessments

A total of 119 older adults were enrolled in the present study: 16 healthy controls (4 men and 12 women; mean age, 71.31 $\pm$ 5.06 years), 57 individuals with preMetS (29 men and 28 women; mean age, 72.44 $\pm$ 5.82 years), and 46 individuals with MetS (27 men and 19 women; mean age, 72.15 $\pm$ 4.97 years). There were no differences in age; sex; years of education; Brinkman index of cigarette consumption cumulative amount; handedness; total cholesterol; low-density lipoprotein (LDL) cholesterol; mean CAVI; Fazekas scale (periventricular and deep WM); locomotive syndrome stage; or the MOCA-J, MMSE, TMT (B–A), GDS-15-J, and GLFS-25 scores among the groups. No significant differences were observed between healthy controls and individuals with preMetS for HDL cholesterol, triglycerides, fasting plasma glucose, HbA1c, HOMA-IR, and standardized two-step test score, or between individuals with preMetS and MetS for systolic and diastolic blood pressures and stand-up test score.

Individuals with preMetS and MetS showed significantly ($P < 0.05$) higher values for body mass index, waist circumference, systolic and diastolic blood pressures, subcutaneous and visceral fat areas, and lower stand-up test scores than healthy controls. Individuals with MetS showed significantly lower HDL cholesterol and standardized two-step test scores, and higher triglycerides, fasting plasma glucose, HbA1c, and HOMA-IR than healthy controls. Furthermore, individuals with MetS had significantly lower HDL cholesterol and higher body mass index, waist circumference, triglyceride level, fasting plasma glucose, HbA1c, HOMA-IR, subcutaneous and visceral fat areas, and two-step test scores than those with preMetS.

3.2. Whole-brain fixel-based analysis

Compared with healthy controls, individuals with MetS had significantly (FWE-corrected $P < 0.05$) lower FD in the splenium of the CC and right posterior limb of the internal capsule, lower log-FC in the left CST, bilateral mammillothalamic tract, cerebral peduncle, and SCP, and lower FDC in the bilateral CST, mammillothalamic tract, MCP, and SCP (Figure 3). No significant differences were observed in any of the fixel-based metrics between healthy controls and individuals with preMetS or between individuals with preMetS and MetS.

3.3. Fixel-wise tract of interest analysis

Individuals with MetS and preMetS showed significantly (FWE-corrected $P < 0.05$ following FDR correction) reduced FD (Figure 4) in the ATR (left), CST (bilateral), SCP (bilateral), and splenium of the CC than healthy controls, and the differences were relatively more pronounced in those with MetS. Individuals with MetS showed significantly reduced log-FC (Figure 5) in the ATR (left), CST (bilateral), ICP (bilateral), MCP, SCP (bilateral), and SLF-I (left) compared with healthy controls. Individuals with MetS also showed a significantly reduced FDC (Figure 6) in the ATR (left), CST (bilateral), ICP (left), IFO (left), MCP, and SCP (bilateral) compared with healthy controls. No significant differences were observed for FDC or log-FC between healthy controls and

Table 1 — Demographics and clinical characteristics of the participants.

	HCs (N = 16)	preMetS (N = 57)	MetS (N = 46)	*P*-values			
				HC vs. preMetS vs. MetS	HC vs. preMetS	HC vs. MetS	preMetS vs. MetS
Sex, n (male/female)[a]	4/12	29/28	27/19	0.067			
Age (years)[c]	71.31 ± 5.06	72.44 ± 5.82	72.15 ± 4.97	0.841			
Years of education[c]	14.50 ± 1.90	14.74 ± 2.41	14.11 ± 2.00	0.355			
Brinkman index[c]	73.13 ± 209.66	310.74 ± 551.57	365.02 ± 571.26	0.072			
Handedness, n (left/right/mixed)[a]	0/14/2	3/51/3	9/45/3	0.197			
MetS-related characteristics:							
BMI (kg/m^2)[b]	19.80 ± 2.30	22.80 ± 2.24	24.68 ± 2.42	**<0.001**	**<0.001**	**<0.001**	**<0.001**
Waist circumference (cm)[c]	76.63 ± 7.80	83.81 ± 5.97	93.28 ± 7.65	**<0.001**	**0.002**	**<0.001**	**<0.001**
Systolic blood pressure (mmHg)[b]	116.94 ± 8.68	137.88 ± 15.16	141.76 ± 15.42	**<0.001**	**<0.001**	**<0.001**	0.374
Diastolic blood pressure (mmHg)[b]	78.19 ± 6.65	86.18 ± 8.55	88.78 ± 8.62	**<0.001**	**0.003**	**<0.001**	0.261
Total cholesterol (mg/dL)[c]	196.25 ± 34.61	200.33 ± 32.29	213.43 ± 53.86	0.347			
HDL cholesterol (mg/dL)[c]	71.25 ± 14.98	64.53 ± 14.75	59.50 ± 12.58	**0.008**	0.105	**0.006**	**0.030**
LDL cholesterol (mg/dL)[b]	108.63 ± 24.30	116.40 ± 28.50	125.26 ± 33.81	0.122			
Triglycerides (mg/dL)[c]	68.44 ± 21.65	93.39 ± 51.93	129.26 ± 81.83	**<0.001**	0.058	**<0.001**	**0.002**
Fasting plasma glucose (mg/dL)[c]	90.56 ± 5.44	95.40 ± 9.77	107.00 ± 15.14	**<0.001**	0.084	**<0.001**	**<0.001**
HbA1c (mmol/mol)[c]	5.51 ± 0.25	5.73 ± 0.47	5.92 ± 0.58	**0.005**	0.161	**0.001**	**0.037**
HOMA-IR index[c]	0.75 ± 0.41	1.06 ± 0.80	1.68 ± 0.87	**<0.001**	0.070	**<0.001**	**<0.001**
Visceral fat area (cm^2)[c]	47.09 ± 27.71	72.07 ± 26.27	101.28 ± 42.42	**<0.001**	**0.002**	**<0.001**	**<0.001**
Subcutaneous fat area (cm^2)[b]	103.72 47.56	140.64 53.04	169.89 46.17	**<0.001**	**0.027**	**<0.001**	**0.010**
Arteriosclerosis measure:							
Bilateral CAVI[b]	8.59 ± 1.06	8.97 ± 1.21	9.21 ± 0.84	0.126			
Neuropsychological measures:							
MOCA-J[c]	25.94 ± 1.91	25.75 ± 2.73	25.26 ± 2.79	0.669			
MMSE[c]	28.56 ± 1.31	28.05 ± 1.62	28.22 ± 1.13	0.542			
TMT (B−A; seconds)[c]	66.69 ± 23.90	68.47 ± 38.36	75.30 ± 47.87	0.790			
GDS-15-J[c]	1.44 ± 1.55	1.81 ± 1.81	2.26 ± 1.96	0.238			
Locomotor function tests:							
Stage, N (0/1/2)[a]	7/8/1	15/31/11	7/32/7	0.149			
Stand-up test[c]	4.56 ± 0.63	3.95 ± 1.20	3.63 ± 0.93	**0.004**	**0.036**	**<0.001**	0.115
Standardized two-step test[c]	1.45 ± 0.10	1.38 ± 0.15	1.32 ± 0.13	**0.006**	0.127	**0.002**	**0.035**
GLF-S 25[c]	6.31 ± 7.25	6.60 ± 7.84	6.74 ± 7.11	0.722			
Fazekas scale:							
Periventricular WM, N (0/1/2/3)[a]	0/14/2/0	0/46/11/0	1/39/6/0	0.655			
Deep WM, N (0/1/2/3)[a]	0/13/2/1	1/39/15/2	0/35/10/1	0.792			

Data are presented in mean ± standard deviation unless otherwise stated. Statistical analyses were performed using χ^2 test[a], one-way analysis of variance with Tukey's Honest Significant Difference post hoc test[b], and Kruskal—Wallis with post hoc Mann—Whitney test[c]. Bold values denote statistical significance ($P < 0.05$).

BMI, body mass index; CAVI, cardio-ankle vascular index; HCs, healthy controls; HDL, high-density lipoprotein; HbA1c, glycated hemoglobin A1c; GDS-15-J, Japanese version of the 15-item Geriatric Depression Scale; GLF-S 25, 25-question geriatric locomotive function scale; HOMA-IR, homeostasis model assessment of insulin resistance; LDL, low-density lipoprotein; MetS, metabolic syndrome; MOCA-J, Japanese version of Montreal cognitive assessment; MMSE, mini-mental state examination; preMetS, premetabolic syndrome; TMT (B−A), the difference between time in seconds spent in completing parts B and A of the trail-making test; WM, white matter.

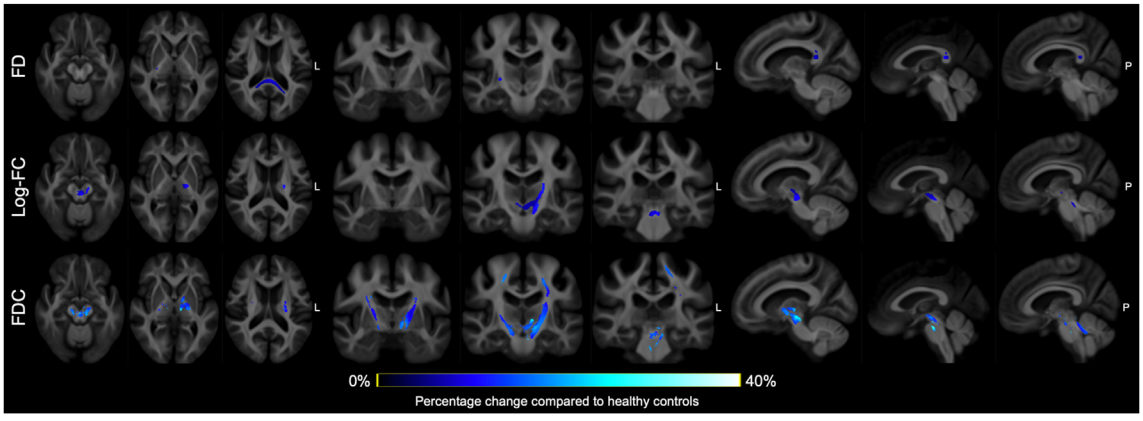

Figure 3: Fiber tract-specific reductions in individuals with metabolic syndrome compared to healthy controls from whole-brain fixel-based analysis. Streamline segments (blue) were cropped from the template tractogram to include only streamline points corresponding to significant fixels (Family-wise error-corrected $P < 0.05$) and colored according to the percentage effect decrease in patients with metabolic syndrome compared with healthy controls. FD, fiber density; FDC, fiber density and cross-section; log-FC, log-transformed fiber-bundle cross-section.

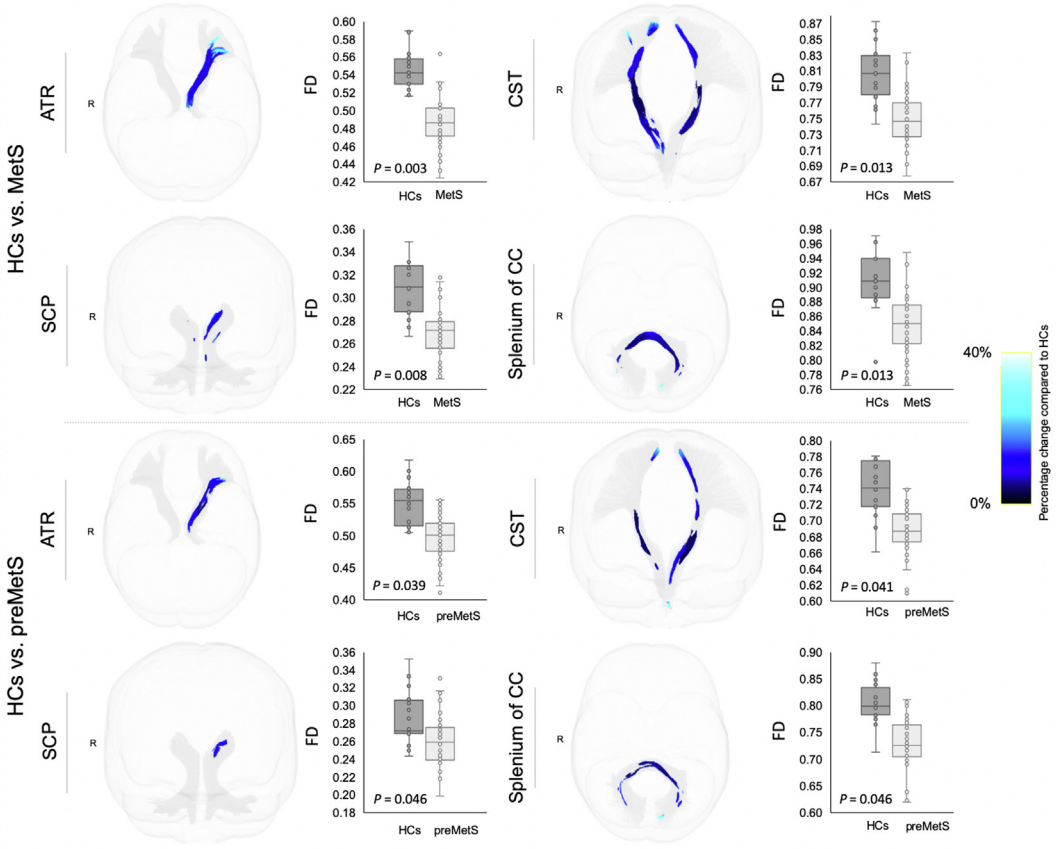

Figure 4: White matter tracts showing reduced fiber density (FD) in individuals with premetabolic syndrome (preMetS) or metabolic syndrome (MetS) compared with healthy controls (HCs). Tract-specific streamline segments (blue) represent streamlines corresponding to significant fixels (Family-wise error [FWE]-corrected $P < 0.05$) and are colored according to the percentage effect decrease in individuals with preMetS (upper panel) or MetS (lower panel) compared with HCs. Boxplots illustrate within-group variability (calculated across all significant fixels). The bottom and top of the box represent the first and third quartiles, respectively, and the band inside the box represents the median. Whiskers represent the maximum and minimum values of all data. FWE-corrected *P*-values are shown at the peak fixel level of each tract after false discovery rate correction. ATR, anterior thalamic radiation; CC, corpus callosum; CST, corticospinal tract; SCP, superior cerebellar peduncle.

individuals with preMetS or any of the fixel-based metrics between individuals with preMetS and MetS.

We observed a significant (FDR-adjusted $P < 0.05$) correlation between increased Brinkman index and reduced FD in the MCP and splenium of the CC (Table 2). Significant negative correlations were also observed between log-FC and FDC metrics and waist circumference, LDL cholesterol, and TMT (B—A) scores. Specifically, associations were demonstrated between increased waist circumference and reduced log-FC in the AF, ATR, cingulum, CST, IFO, ILF, SLF-I, SLF-II, SLF-III, and UF or lower FDC in the AF, ATR, cingulum, IFO, ILF, SLF-I, SLF-II, SLF-III, and UF; between higher LDL cholesterol and lower log-FC in the CST, ICP, IFO, ILF, MCP, SCP, and UF or FDC in the ICP, ILF, and UF; and between higher TMT (B—A) scores and lower log-FC in the AF, ATR, cingulum, CST, ICP, IFO, ILF, MCP, SCP, SLF-I, SLF-II, SLF-III, and UF or lower FDC in the ATR, cingulum, CST, ICP, MCP, and SCP.

3.4. Tract-based spatial statistics analysis

There were no significant differences in FA and MD among all groups.

4. DISCUSSION

In the present study, we applied FBA to investigate WM fiber tract-specific in older adults with preMetS and MetS. Individuals with MetS exhibit extensive axonal loss and fiber-bundle atrophy within WM pathways considered critical to cognitive and motor functions, which are largely congruent with the regions of WM abnormalities previously reported in MetS [7] or individual components of MetS [2]. Meanwhile, individuals with preMetS showed subtle axonal loss without evidence of morphological alterations to the fiber bundle. Our findings also showed evidence of associations between MetS-related WM neuronal damage and impairment in executive function, abdominal obesity, hyper-LDL cholesterolemia, or smoking habit.

4.1. Reduced white matter fiber tract-specific in premetabolic syndrome and metabolic syndrome

Although there is limited histological evidence, particularly in WM, lower neuronal cell bodies have been observed in various frontal and temporal areas in the postmortem brain tissue of donors who were obese, a main feature of MetS, compared with normal-weight individuals [47]. In agreement, fixel-wise changes in individuals with preMetS and MetS were identified in the WM tracts that connect parts of the frontal or temporal cortices to other cortical or subcortical areas, such as the ATR, CST, IFO, and SLF-I. Thus, the possibility that the distribution of WM alterations among individuals with preMetS and MetS is a primary effect of WM pathology and/or axonal degeneration associated with cortical neuron injury warrants further investigation.

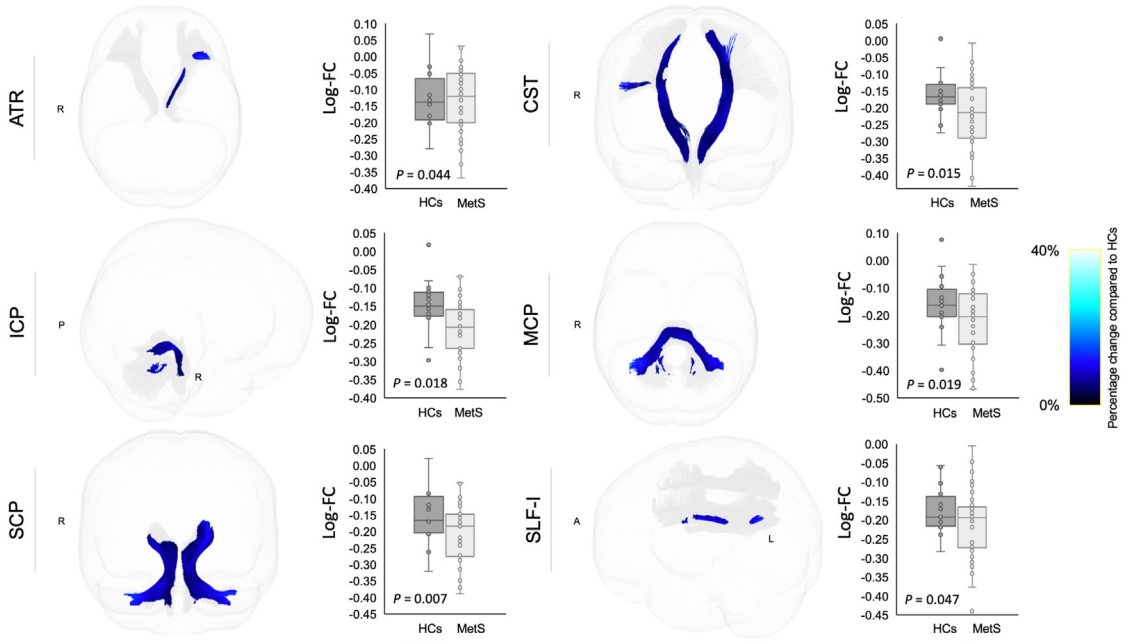

Figure 5: White matter tracts showing reduced log-transformed fiber-bundle cross-section (log-FC) in individuals with metabolic syndrome (MetS) compared with healthy controls (HCs). Tract-specific streamline segments (blue) represent streamlines corresponding to significant fixels (Family-wise error [FWE]-corrected $P < 0.05$) and are colored according to the percentage effect decrease in individuals with MetS compared with HCs. Boxplots illustrate within-group variability (calculated across all significant fixels). The bottom and top of the box represent the first and third quartiles, respectively, and the band inside the box represents the median. Whiskers represent the maximum and minimum values of all data. FWE-corrected *P*-values are shown at the peak fixel level of each tract after false discovery rate correction. ATR, anterior thalamic radiation; CST, corticospinal tract; ICP, inferior cerebellar peduncle; MCP, middle cerebellar peduncle; SCP, superior cerebellar peduncle; SLF, superior longitudinal fasciculus.

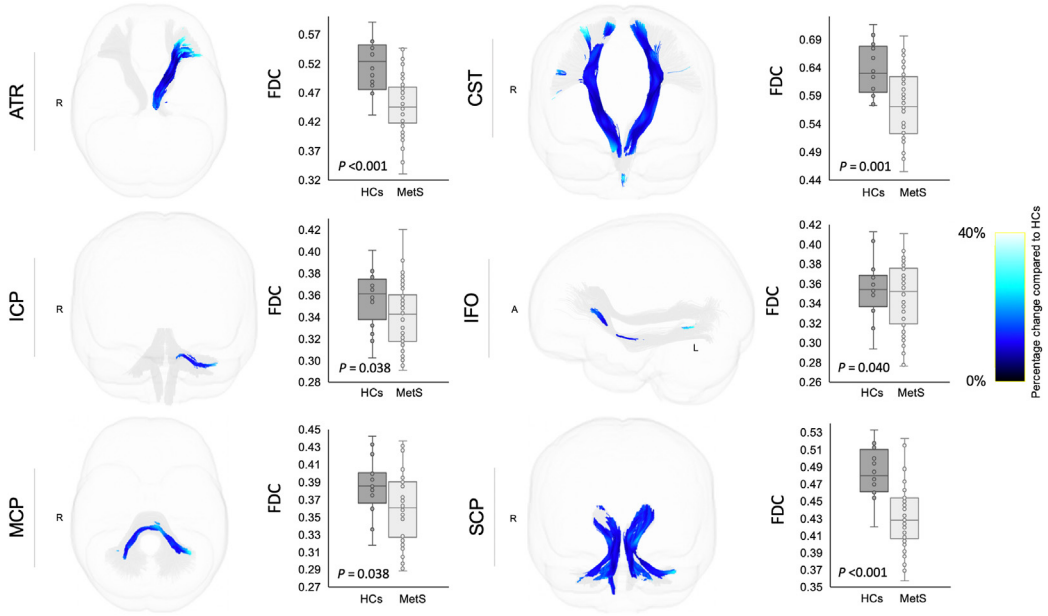

Figure 6: White matter tracts showing reduced fiber density and cross-section (FDC) in individuals with metabolic syndrome (MetS) compared with healthy controls (HCs). Tract-specific streamline segments (blue) represent streamlines corresponding to significant fixels (Family-wise error [FWE]-corrected $P < 0.05$) and are colored according to the percentage effect decrease in individuals with MetS compared with HCs. Boxplots illustrate within-group variability (calculated across all significant fixels). The bottom and top of the box represent the first and third quartiles, respectively, and the band inside the box represents the median. Whiskers represent maximum and minimum values of all data. FWE-corrected *P*-values are shown at the peak fixel level of each tract after false discovery rate correction. ATR, anterior thalamic radiation; CST, corticospinal tract; ICP, inferior cerebellar peduncle; IFO, inferior fronto-occipital fasciculus; MCP, middle cerebellar peduncle; SCP, superior cerebellar peduncle.

Our observations in individuals with preMetS and MetS indicated substantial axonal loss (i.e. reduced FD) in the ATR, CST, SCP, and splenium of the CC compared with healthy controls, with relatively greater effect sizes observed in individuals with MetS. FBA also enabled the identification of fiber-bundle atrophy (i.e., reduced log-FC) only in individuals with MetS. Notably, fiber tract-specific atrophy was

Table 2 — Significant associations between fixel-based metrics and clinical scores in individuals with preMetS and MetS.

	Brinkman index		Waist circumference				LDL cholesterol				TMT (B—A)			
	FD		Log-FC		FDC		Log-FC		FDC		Log-FC		FDC	
	P	r	*P*	r	*P*	r	*P*	r	*P*	r	*P*	r	*P*	r
AF	0.565	−0.15	**<0.001**	−0.37	**0.009**	−0.32	0.062	−0.19	0.162	−0.15	**0.004**	−0.31	0.057	−0.20
ATR	0.928	−0.02	**<0.001**	−0.37	**0.009**	−0.30	0.059	−0.21	0.101	−0.22	**0.006**	−0.28	**0.015**	−0.29
Cingulum	0.565	−0.15	**0.005**	−0.29	**0.013**	−0.28	0.059	−0.21	0.162	−0.15	**0.004**	−0.31	**0.015**	−0.28
CST	0.565	−0.13	**0.012**	−0.26	0.078	−0.19	**0.031**	−0.25	0.121	−0.18	**0.004**	−0.32	**0.020**	−0.27
ICP	0.090	−0.36	0.677	−0.04	0.583	−0.06	**0.008**	−0.33	**0.034**	−0.27	**0.005**	−0.30	**0.026**	−0.25
IFO	0.289	−0.25	**0.005**	−0.30	**0.032**	−0.23	**0.041**	−0.23	0.121	−0.19	**0.004**	−0.32	0.054	−0.22
ILF	0.617	0.11	**0.005**	−0.30	**0.009**	−0.29	**0.031**	−0.26	**0.034**	−0.27	**0.011**	−0.26	0.223	−0.13
MCP	**0.028**	−0.43	0.591	−0.06	0.583	−0.06	**0.031**	−0.25	0.121	−0.18	**0.004**	−0.32	**0.015**	−0.30
SCP	0.091	−0.34	0.390	−0.10	0.304	−0.11	**0.011**	−0.30	0.121	−0.18	**0.004**	−0.31	**0.015**	−0.29
SLF-I	0.565	−0.13	**0.002**	−0.34	**0.009**	−0.30	0.062	−0.19	0.121	−0.18	**0.004**	−0.31	0.054	−0.21
SLF-II	0.565	−0.17	**<0.001**	−0.37	**0.020**	−0.26	0.062	−0.20	0.211	−0.13	**0.011**	−0.26	0.057	−0.20
SLF-III	0.843	−0.06	**0.009**	−0.27	**0.023**	−0.25	0.158	−0.14	0.211	−0.13	**0.021**	−0.23	0.067	−0.19
Splenium of the CC	**0.013**	−0.49	0.083	−0.19	0.186	−0.15	0.087	−0.18	0.152	−0.16	0.093	−0.17	0.564	−0.06
UF	0.928	−0.01	**0.002**	−0.33	**0.009**	−0.30	**0.008**	−0.32	**0.034**	−0.28	**0.006**	−0.28	0.054	−0.21

The table shows FDR-adjusted *P*-value and partial correlation coefficient (r). Bold values denote statistical significance at the FDR-adjusted $P < 0.05$. AF, arcuate fasciculus; ATR, anterior thalamic radiation; CC, corpus callosum; CST, cingulum, corticospinal tract; FD, fiber density; FDC, fiber density and cross-section; ICP, inferior cerebellar peduncle; IFO, inferior fronto-occipital fasciculus; ILF, inferior longitudinal fasciculus; LDL, low-density lipoprotein; log-FC, log-transformed fiber-bundle cross-section; MCP, middle cerebellar peduncle; MetS, metabolic syndrome; preMetS, premetabolic syndrome; SCP, superior cerebellar peduncle; SLF, superior longitudinal fasciculus; TMT (B—A), the difference between time in seconds spent in completing parts B and A of the trail-making test; UF, uncinate fasciculus.

observed spatially more extensive, including in regions with loss of FD, ICP, MCP, and SLF-I. As expected, individuals with MetS showed reduced FDC overlap with regions with significantly reduced FD and FC, with relatively larger effect sizes than the changes in FD or log-FC alone. FDC combines the information of microstructural differences in FD and morphological changes in FC, thus enabling a more sensitive assessment of fixel-wise effects [11].

The dissociable results of fixel-based metrics in individuals with preMetS (only reduced FD) and MetS (reduced in all fixel metrics) indicated that different WM tracts are affected differently or show different stages of neurodegeneration. FD provides a measure approximately proportional to axons present within a voxel and depends on axons as well as the nonaxonal space or volume in between [11]. It was suggested that the number of axons or their individual volume within the fiber-specific tract may be reduced in the earlier stages of degeneration, but the macroscopic FC remains unchanged if extracellular area and matrix related to gliosis or inflammation filled the additional extra-axonal space. The fiber bundle becomes atrophic after the debris is cleared [9,48], implying that axonal loss could precede fiber-bundle atrophy. A longitudinal study of Parkinson's disease, for example, showed reductions in FD between the first follow-up assessment and baseline, whereas FC only decreased between the second and first follow-up assessment [17]. Our findings also suggest that log-FC and FDC were reduced without changes in FD in individuals with MetS compared with healthy controls, noticeably in the ICP and MCP. In some cases, if degeneration is followed by atrophy (i.e., reduced FC), the within-voxel FD for the remaining axons may suggest an increase in FD, resulting in insignificant results in between-group comparisons [9]. Nevertheless, since reduced FDC, which is a combined measure of FD and FC, was also observed, it is reasonable to assume that the changes in ICP and MCP were driven by both fiber density and bundle cross-sectional size. Collectively, our observations indicate early axonal loss in preMetS and extensive axonal loss as well as fiber-bundle atrophy in MetS. In support of our findings, a previous longitudinal study showed subclinical elevation in MetS risk indicators as predictors of greater WM microstructural damage [49]. Furthermore, axonal atrophy was associated with irreversible disability [48]; thus, detecting axonal loss before atrophy may be necessary for early intervention.

In terms of laterality, changes in fixel metrics were primarily observed in the left hemisphere in some WM tracts. While we have no clear explanation for these observations, we speculate that disorders of the brain vascular system may be related to our findings. Hypertension is known to contribute to vascular damage and plaque formation in cerebral blood vessels [50]. The direct connection of the left carotid artery to the aortic arch has been shown to cause higher arterial pressure, which leads to greater vulnerability of atherosclerotic disease in the left carotid artery [51]. In a recent study involving elderly individuals with hypertension, abnormalities in the perivascular space diffusion signal, indicating brain clearance dysfunction, were observed in the left hemisphere only [52]. Nevertheless, some changes were also observed bilaterally, indicating that the pathological processes in MetS are complex and involve multiple mechanisms that need further exploration.

4.2. Effects of metabolic syndrome on executive and locomotor functions

Our results revealed significant associations between fiber density and bundle cross-sectional reductions and executive dysfunction in individuals with preMetS and MetS, as indicated by prolonged time to complete TMT (B—A), in WM tracts important for executive function [53], such as ATR, cingulum, IFO, ILF, and SLF. The WM microstructural damage, such as lower FA and/or higher MD, has also been associated with impairment in executive function in patients with individual components of MetS, such as hyperglycemia [54], hypertension [55], and obesity [56]. However, in contrast to DTI, FBA may provide more detailed biological information on changes occurring in the WM structure related to executive dysfunction in MetS. It is worth noting that we found no significant difference in TMT (B—A) scores between groups, which could suggest that that WM changes gradually and begins long before symptoms emerge. Accordingly, our findings indicated fixel-based metrics as promising early biomarkers of executive dysfunction in MetS.

Furthermore, we observed poorer locomotor function in individuals with MetS compared with healthy controls and individuals with

preMetS, as indicated by both stand-up and two-step tests. Locomotor dysfunction was also found in individuals with preMetS, but was less severe, as reflected by a significantly lower score in the stand-up test compared with that of healthy controls. In support of this observation, FBA revealed that all fixel-based metrics were reduced in individuals with MetS and FD was reduced in individuals with preMetS in WM tracts crucial for motor functions, such as CST and cerebellar peduncles [57,58]. Similarly, previous DTI studies also observed lower FA and/or higher MD in the CST and cerebellar peduncles individuals with obesity; however, locomotor scores were not evaluated [59–62]. Unexpectedly, we were unable to detect significant correlations between fixel-based metrics and all locomotor function tests, likely due to the influence of other components of locomotor functions, such as musculoskeletal and peripheral nervous systems, on the tests. Nevertheless, FBA may indicate that locomotor dysfunction in MetS was related, at least in part, to WM degenerative process.

4.3. Modifiable lifestyle variables associated with white matter neural tissue microstructure in metabolic syndrome

Higher waist circumference was associated with reduced log-FC or FDC for approximately all WM tracts in individuals with preMetS and MetS. However, unexpectedly, Birdsill et al. [63] found that higher FA was significantly associated with higher waist circumference. DTI cannot resolve crossing fibers accurately; thus, higher FA may reflect selective neurodegeneration or compensatory WM microstructural reorganization [15]. Alternatively, the CSD model can accurately resolve different fiber orientations within a voxel of interest [11], providing a more reliable measurement. Waist circumference is a common indicator of abdominal fat accumulation [64], which is a major feature of MetS. The Japanese waist circumference threshold is influenced by both visceral and subcutaneous fat [26]. A large study involving Japanese participants revealed that visceral and subcutaneous adipose tissue accumulation was associated with insulin resistance [65]. Abdominal obesity-induced neuroinflammation and brain insulin resistance are associated with breakdown of the blood–brain barrier [66] and reduced intraneuronal glucose metabolism, respectively, in MetS [67], and have been suggested as the pathological features underlying WM neurodegeneration. However, we did not find any evidence of a direct association between insulin resistance, as indexed by HOMA-IR, and WM microstructure. Higher HOMA-IR was correlated with lower brain glucose metabolism, as observed using fluorodeoxyglucose positron emission tomography; however, this association has only been detected in amyloid-positive patients [68]. Accordingly, future studies should use fixel-based measures to clarify the relationship between MetS and Alzheimer's disease.

We observed that higher levels of LDL cholesterol negatively impact WM microstructure, as indicated by lower log-FC or FDC. Our findings were consistent with those from previous studies that evaluated associations between serum lipid levels and DTI measurements in the WM of healthy adults [69,70]. For instance, increased levels of LDL cholesterol were correlated with reduced FA and LDL cholesterol had the largest number of voxels, showing significant associations with FA, compared to other lipid measurements (HDL cholesterol, triglycerides, and total cholesterol) [70]. LDL cholesterol represents 60%–70% of circulating serum cholesterol and is considered to be the major atherogenic lipoprotein and risk factor for vascular-based disease. Thus, LDL cholesterol potentially influenced WM microstructure by promoting intracranial atherosclerosis and brain chronic hypoperfusion [71].

Finally, we noted an inverse relationship between FD and Brinkman index, which reflects cumulative cigarette consumption, in the splenium of CC. Our findings are concordant with those of previous studies that demonstrated a significant correlation between reduced FA in the CC and tobacco consumption [72] and duration of cigarette smoking [73]. A previous study showed that smokers were relatively more insulin-resistant than nonsmokers and that smoking mediates endothelial dysfunction associated with reduced arterial compliance and increases arterial stiffness [74].

4.4. Advantages of fixel-based over tensor-derived metrics

To date, scarce data are available regarding the effects of MetS on WM neural tissue microstructure using DTI, particularly in older adults with MetS, and the findings of previous studies are inconsistent. Segura et al. [6] observed compromised WM microstructure (as indexed by lower FA and higher MD) occurring predominantly in the anterior parts of the CC, ILF, SLF, and UF in individuals with MetS compared with healthy controls. In contrast, the results of the study by Sala et al. [75] and the present study showed no significant differences in FA and MD between individuals with preMetS or MetS and healthy controls. This discrepancy may be due to the differences in the criteria used to define MetS as well as study sample characteristics. The inconsistencies in DTI findings may also be attributable to the limitations of the tensor-derived metrics in regions with crossing fibers. In contrast to the findings of the study by Segura et al. [6], we did not observe differences in the anterior–posterior gradient using FBA. Indeed, Segura et al. reported that WM regions exhibit significant changes in DTI metrics, such as CC and SLF [6], and have been found to contain a relatively higher number of crossing fibers per voxel, suggesting unreliable interpretation of DTI-associated metrics [4].

In accordance with the study by Sala et al. [75], we were unable to demonstrate WM microstructural changes in individuals with preMetS using DTI. This may indicate that fixel-based metrics have a higher sensitivity than DTI in detecting early axon changes, as was also shown previously in studies in neurodegenerative diseases, such as Alzheimer's disease [14], Parkinson's disease [15,18], and multiple sclerosis [48] This fixel-based approach allows us to differentiate between changes in microstructural FD and macrostructural FC; thus, provides greater sensitivity in detecting groupwise differences in preMetS, particularly in crossing fiber regions.

4.5. Study limitations and future directions

The present study has some limitations. Although we included more older adults with MetS than previous studies (Segura et al. [6], $n = 19$, and Sala et al. [75], $n = 18$), the present study had a small sample size ($n = 46$) in relation to the prevalence of MetS and may have limited statistical power. This might have led to false-positive or false-negative results. Furthermore, the cross-sectional study design of the study limited our ability to examine degenerative changes in WM over the progression of preMetS and MetS. Future studies with larger sample sizes investigating the longitudinal trajectory of individuals with preMetS who progress to MetS are likely to provide further insight into the association between clinical trajectory and degenerative changes in particular fiber pathways.

The prevalence of MetS varies and depends on the MetS criteria used [20] as well as the ethnic group. In the present study, we only included Japanese elderly living in urban areas and adjusted the waist circumference threshold for our Japanese cohort. Further studies are required to investigate changes in WM in MetS defined using different criteria in different ethnicities.

Finally, MetS has been liked with a higher WM hyperintensity load [76]. Although the present study showed no statistical differences in periventricular and deep WM Fazekas scales between all groups and correlation analysis with fixel-based metrics, the presence of these

lesions may be associated with decreases in fixel-wise metrics [77]. Future studies are required to investigate the association of fixel-based metrics and WM lesions.

4.6. Conclusions

Our findings suggest that individuals with MetS have a characteristic pattern of WM fiber tract degeneration, involving WM pathways considered crucial for cognitive and motor functions, that manifests as both axonal loss and atrophy, whereas individuals with preMetS show earlier WM degenerative process that manifests as reduced FD without fiber-bundle morphology changes. Furthermore, we confirmed the negative impact of MetS on executive function performance associated with compromised WM neural tissue microstructure. Finally, our findings indicate that optimal management of modifiable variables, such as abdominal obesity, hyper-LDL-cholesterolemia, and smoking habits, are necessary to maintain WM neural health in older adults.

DATA STATEMENT

The data that support the findings of this study are available on request from the corresponding author.

AUTHOR CONTRIBUTIONS

Christina Andica: Conceptualization; Methodology; Formal analysis, Visualization, and Writing - original draft. **Koji Kamagata:** Conceptualization, Methodology; and Writing - review & editing, and Funding acquisition. **Wataru Uchida, Kaito Takabayashi, and Keigo Shimoji:** Formal analysis, Visualization, and Writing – review & editing. **Hideyoshi Kaga, Yuki Someya, Yoshifumi Tamura, Ryuzo Kawamori, Hirotaka Watada, and Masaaki Hori:** Conceptualization, Methodology, Supervision, Writing - review & editing. **Shigeki Aoki:** Conceptualization, Writing - review & editing, Supervision, and Funding acquisition.

FUNDING

This study was partially supported by the Juntendo Research Branding Project; the Japan Society for the Promotion of Science (JSPS) Grants-in-Aid for Scientific Research (KAKENHI; Grant numbers JP21K07690, 20F20113, JP18H02772, and 19K17244); a Grant-in-Aid for Special Research in Subsidies for ordinary expenses of private schools from The Promotion and Mutual Aid Corporation for Private Schools of Japan; and the Brain/MINDS Beyond program of the Japan Agency for Medical Research and Development (Grant number JP19dm0307101).

CONFLICT OF INTEREST

None.

APPENDIX A. SUPPLEMENTARY DATA

Supplementary data to this article can be found online at https://doi.org/10.1016/j.molmet.2022.101527.

REFERENCES

[1] Alberti, K.G., Eckel, R.H., Grundy, S.M., Zimmet, P.Z., Cleeman, J.I., Donato, K.A., et al., 2009. Harmonizing the metabolic syndrome: a joint interim statement of the International Diabetes Federation Task Force on Epidemiology and Prevention; National Heart, Lung, and Blood Institute; American Heart Association; World Heart Federation; International Atherosclerosis Society; and International Association for the Study of Obesity. Circulation 120(16):1640–1645.

[2] Alfaro, F.J., Gavrieli, A., Saade-Lemus, P., Lioutas, V.A., Upadhyay, J., Novak, V., 2018. White matter microstructure and cognitive decline in metabolic syndrome: a review of diffusion tensor imaging. Metabolism 78: 52–68.

[3] Nakamura, M., Kobashi, Y., Hashizume, H., Oka, H., Kono, R., Nomura, S., et al., 2016. Locomotive syndrome is associated with body composition and cardiometabolic disorders in elderly Japanese women. BMC Geriatrics 16(1):166.

[4] Jeurissen, B., Leemans, A., Tournier, J.D., Jones, D.K., Sijbers, J., 2013. Investigating the prevalence of complex fiber configurations in white matter tissue with diffusion magnetic resonance imaging. Human Brain Mapping 34(11):2747–2766.

[5] Andica, C., Kamagata, K., Hatano, T., Saito, Y., Ogaki, K., Hattori, N., et al., 2020. MR biomarkers of degenerative brain disorders derived from diffusion imaging. Journal of Magnetic Resonance Imaging 52(6):1620–1636.

[6] Segura, B., Jurado, M.A., Freixenet, N., Falcón, C., Junqué, C., Arboix, A., 2009. Microstructural white matter changes in metabolic syndrome: a diffusion tensor imaging study. Neurology 73(6):438–444.

[7] Shimoji, K., Abe, O., Uka, T., Yasmin, H., Kamagata, K., Asahi, K., et al., 2013. White matter alteration in metabolic syndrome: diffusion tensor analysis. Diabetes Care 36(3):696–700.

[8] Raffelt, D.A., Smith, R.E., Ridgway, G.R., Tournier, J.D., Vaughan, D.N., Rose, S., et al., 2015. Connectivity-based fixel enhancement: whole-brain statistical analysis of diffusion MRI measures in the presence of crossing fibres. Neuroimage 117:40–55.

[9] Raffelt, D.A., Tournier, J.D., Smith, R.E., Vaughan, D.N., Jackson, G., Ridgway, G.R., et al., 2017. Investigating white matter fibre density and morphology using fixel-based analysis. Neuroimage 144(Pt A):58–73.

[10] Jeurissen, B., Tournier, J.D., Dhollander, T., Connelly, A., Sijbers, J., 2014. Multi-tissue constrained spherical deconvolution for improved analysis of multi-shell diffusion MRI data. Neuroimage 103:411–426.

[11] Dhollander, T., Clemente, A., Singh, M., Boonstra, F., Civier, O., Duque, J.D., et al., 2021. Fixel-based analysis of diffusion MRI: methods, applications, challenges and opportunities. Neuroimage 241:118417.

[12] Choy, S.W., Bagarinao, E., Watanabe, H., Ho, E.T.W., Maesawa, S., Mori, D., et al., 2020. Changes in white matter fiber density and morphology across the adult lifespan: a cross-sectional fixel-based analysis. Human Brain Mapping 41(12):3198–3211.

[13] Zivari Adab, H., Chalavi, S., Monteiro, T.S., Gooijers, J., Dhollander, T., Mantini, D., et al., 2020. Fiber-specific variations in anterior transcallosal white matter structure contribute to age-related differences in motor performance. Neuroimage 209:116530.

[14] Mito, R., Raffelt, D., Dhollander, T., Vaughan, D.N., Tournier, J.D., Salvado, O., et al., 2018. Fibre-specific white matter reductions in Alzheimer's disease and mild cognitive impairment. Brain 141(3):888–902.

[15] Andica, C., Kamagata, K., Saito, Y., Uchida, W., Fujita, S., Hagiwara, A., et al., 2021. Fiber-specific white matter alterations in early-stage tremor-dominant Parkinson's disease. NPJ Parkinson's Disease 7(1):51.

[16] Li, Y., Guo, T., Guan, X., Gao, T., Sheng, W., Zhou, C., et al., 2020. Fixel-based analysis reveals fiber-specific alterations during the progression of Parkinson's disease. Neuroimage: Clinical 27:102355.

[17] Rau, Y.A., Wang, S.M., Tournier, J.D., Lin, S.H., Lu, C.S., Weng, Y.H., et al., 2019. A longitudinal fixel-based analysis of white matter alterations in patients with Parkinson's disease. Neuroimage: Clinical 24:102098.

[18] Zarkali, A., McColgan, P., Leyland, L.A., Lees, A.J., Rees, G., Weil, R.S., 2020. Fiber-specific white matter reductions in Parkinson hallucinations and visual dysfunction. Neurology 94(14):e1525–e1538.

[19] Koizumi, K., Oku, M., Hayashi, S., Inujima, A., Shibahara, N., Chen, L., et al., 2019. Identifying pre-disease signals before metabolic syndrome in mice by dynamical network biomarkers. Scientific Reports 9(1):8767.
[20] Kassi, E., Pervanidou, P., Kaltsas, G., Chrousos, G., 2011. Metabolic syndrome: definitions and controversies. BMC Medicine 9:48.
[21] [Definition and the diagnostic standard for metabolic syndrome–committee to evaluate diagnostic standards for metabolic syndrome]. Nihon Naika Gakkai Zasshi 94(4), 2005:794—809.
[22] Vidigal Fde, C., Ribeiro, A.Q., Babio, N., Salas-Salvadó, J., Bressan, J., 2015. Prevalence of metabolic syndrome and pre-metabolic syndrome in health professionals: LATINMETS Brazil study. Diabetology & Metabolic Syndrome 7:6.
[23] Someya, Y., Tamura, Y., Kaga, H., Nojiri, S., Shimada, K., Daida, H., et al., 2019. Skeletal muscle function and need for long-term care of urban elderly people in Japan (the Bunkyo Health Study): a prospective cohort study. BMJ Open 9(9):e031584.
[24] Ideno, Y., Takayama, M., Hayashi, K., Takagi, H., Sugai, Y., 2012. Evaluation of a Japanese version of the Mini-Mental State Examination in elderly persons. Geriatrics and Gerontology International 12(2):310—316.
[25] Sugishita, K., Sugishita, M., Hemmi, I., Asada, T., Tanigawa, T., 2017. A validity and reliability study of the Japanese version of the Geriatric Depression Scale 15 (GDS-15-J). Clinical Gerontologist 40(4):233—240.
[26] Matsuzawa, Y., 2005. Metabolic syndrome–definition and diagnostic criteria in Japan. Journal of Atherosclerosis and Thrombosis 12(6):301.
[27] Gomi, T., Kawawa, Y., Nagamoto, M., Terada, H., Kohda, E., 2005. Measurement of visceral fat/subcutaneous fat ratio by 0.3 tesla MRI. Radiation Medicine 23(8):584—587.
[28] Shirai, K., Utino, J., Otsuka, K., Takata, M., 2006. A novel blood pressure-independent arterial wall stiffness parameter; cardio-ankle vascular index (CAVI). Journal of Atherosclerosis and Thrombosis 13(2):101—107.
[29] Matthews, D.R., Hosker, J.P., Rudenski, A.S., Naylor, B.A., Treacher, D.F., Turner, R.C., 1985. Homeostasis model assessment: insulin resistance and beta-cell function from fasting plasma glucose and insulin concentrations in man. Diabetologia 28(7):412—419.
[30] Fujiwara, Y., Suzuki, H., Yasunaga, M., Sugiyama, M., Ijuin, M., Sakuma, N., et al., 2010. Brief screening tool for mild cognitive impairment in older Japanese: validation of the Japanese version of the Montreal Cognitive Assessment. Geriatrics and Gerontology International 10(3):225—232.
[31] Corrigan, J.D., Hinkeldey, N.S., 1987. Relationships between parts A and B of the Trail Making Test. Journal of Clinical Psychology 43(4):402—409.
[32] Nakamura, K., 2008. A "super-aged" society and the "locomotive syndrome". Journal of Orthopaedic Science 13(1):1—2.
[33] Yoshimura, N., Muraki, S., Oka, H., Tanaka, S., Ogata, T., Kawaguchi, H., et al., 2015. Association between new indices in the locomotive syndrome risk test and decline in mobility: third survey of the ROAD study. Journal of Orthopaedic Science 20(5):896—905.
[34] Ogata, T., Muranaga, S., Ishibashi, H., Ohe, T., Izumida, R., Yoshimura, N., et al., 2015. Development of a screening program to assess motor function in the adult population: a cross-sectional observational study. Journal of Orthopaedic Science 20(5):888—895.
[35] Andersson, J.L.R., Skare, S., Ashburner, J., 2003. How to correct susceptibility distortions in spin-echo echo-planar images: application to diffusion tensor imaging. NeuroImage 20(2):870—888.
[36] Veraart, J., Fieremans, E., Novikov, D.S., 2016. Diffusion MRI noise mapping using random matrix theory. Magnetic Resonance in Medicine 76(5):1582—1593.
[37] Andersson, J.L., Sotiropoulos, S.N., 2016. An integrated approach to correction for off-resonance effects and subject movement in diffusion MR imaging. NeuroImage 125:1063—1078.
[38] Tustison, N.J., Avants, B.B., Cook, P.A., Zheng, Y., Egan, A., Yushkevich, P.A., et al., 2010. N4ITK: improved N3 bias correction. IEEE Transactions on Medical Imaging 29(6):1310—1320.
[39] Raffelt, D., Tournier, J.D., Rose, S., Ridgway, G.R., Henderson, R., Crozier, S., et al., 2012. Apparent Fibre Density: a novel measure for the analysis of diffusion-weighted magnetic resonance images. NeuroImage 59(4):3976—3994.
[40] Raffelt, D., Tournier, J.D., Fripp, J., Crozier, S., Connelly, A., Salvado, O., 2011. Symmetric diffeomorphic registration of fibre orientation distributions. NeuroImage 56(3):1171—1180.
[41] Wasserthal, J., Neher, P., Maier-Hein, K.H., 2018. TractSeg - Fast and accurate white matter tract segmentation. NeuroImage 183:239—253.
[42] Fuelscher, I., Hyde, C., Anderson, V., Silk, T.J., 2021. White matter tract signatures of fiber density and morphology in ADHD. Cortex 138:329—340.
[43] Smith, S.M., Jenkinson, M., Johansen-Berg, H., Rueckert, D., Nichols, T.E., Mackay, C.E., et al., 2006. Tract-based spatial statistics: voxelwise analysis of multi-subject diffusion data. NeuroImage 31(4):1487—1505.
[44] Jenkinson, M., Beckmann, C.F., Behrens, T.E., Woolrich, M.W., Smith, S.M., 2012. Fsl. NeuroImage 62(2):782—790.
[45] Dale, A.M., Fischl, B., Sereno, M.I., 1999. Cortical surface-based analysis. I. Segmentation and surface reconstruction. NeuroImage 9(2):179—194.
[46] Smith, R.E., Dhollander, T., Connelly, A., 2019. On the regression of intracranial volume in fixel-based analysis. In: 27th International Society of Magnetic Resonance in Medicine, Montreal, Canada.
[47] Gómez-Apo, E., García-Sierra, A., Silva-Pereyra, J., Soto-Abraham, V., Mondragón-Maya, A., Velasco-Vales, V., et al., 2018. A postmortem study of frontal and temporal gyri thickness and cell number in human obesity. Obesity (Silver Spring) 26(1):94—102.
[48] Gajamange, S., Raffelt, D., Dhollander, T., Lui, E., van der Walt, A., Kilpatrick, T., et al., 2018. Fibre-specific white matter changes in multiple sclerosis patients with optic neuritis. NeuroImage: Clinical 17:60—68.
[49] Bender, A.R., Raz, N., 2015. Normal-appearing cerebral white matter in healthy adults: mean change over 2 years and individual differences in change. Neurobiology of Aging 36(5):1834—1848.
[50] Iadecola, C., Davisson, R.L., 2008. Hypertension and cerebrovascular dysfunction. Cell Metabolism 7(6):476—484.
[51] Selwaness, M., van den Bouwhuijsen, Q., van Onkelen, R.S., Hofman, A., Franco, O.H., van der Lugt, A., et al., 2014. Atherosclerotic plaque in the left carotid artery is more vulnerable than in the right. Stroke 45(11):3226—3230.
[52] Kikuta, J., Kamagata, K., Takabayashi, K., Taoka, T., Yokota, H., Andica, C., et al., 2022. An Investigation of water diffusivity changes along the perivascular space in elderly subjects with hypertension. AJNR. American Journal of Neuroradiology 43(1):48—55.
[53] Loe, I.M., Adams, J.N., Feldman, H.M., 2018. Executive function in relation to white matter in preterm and full term children. Frontiers in Pediatrics 6:418.
[54] Zhang, J., Wang, Y., Wang, J., Zhou, X., Shu, N., Wang, Y., et al., 2014. White matter integrity disruptions associated with cognitive impairments in type 2 diabetic patients. Diabetes 63(11):3596—3605.
[55] Hannesdottir, K., Nitkunan, A., Charlton, R.A., Barrick, T.R., MacGregor, G.A., Markus, H.S., 2009. Cognitive impairment and white matter damage in hypertension: a pilot study. Acta Neurologica Scandinavica 119(4):261—268.
[56] Daoust, J., Schaffer, J., Zeighami, Y., Dagher, A., García-García, I., Michaud, A., 2021. White matter integrity differences in obesity: a meta-analysis of diffusion tensor imaging studies. Neuroscience & Biobehavioral Reviews 129:133—141.
[57] Ramnani, N., 2006. The primate cortico-cerebellar system: anatomy and function. Nature Reviews Neuroscience 7(7):511—522.
[58] Welniarz, Q., Dusart, I., Roze, E., 2017. The corticospinal tract: evolution, development, and human disorders. Developmental Neurobiology 77(7):810—829.
[59] Karlsson, H.K., Tuulari, J.J., Hirvonen, J., Lepomäki, V., Parkkola, R., Hiltunen, J., et al., 2013. Obesity is associated with white matter atrophy: a combined diffusion tensor imaging and voxel-based morphometric study. Obesity (Silver Spring) 21(12):2530—2537.

[60] Kullmann, S., Callaghan, M.F., Heni, M., Weiskopf, N., Scheffler, K., Häring, H.U., et al., 2016. Specific white matter tissue microstructure changes associated with obesity. NeuroImage 125:36–44.

[61] Papageorgiou, I., Astrakas, L.G., Xydis, V., Alexiou, G.A., Bargiotas, P., Tzarouchi, L., et al., 2017. Abnormalities of brain neural circuits related to obesity: a Diffusion Tensor Imaging study. Magnetic Resonance Imaging 37: 116–121.

[62] Verstynen, T.D., Weinstein, A.M., Schneider, W.W., Jakicic, J.M., Rofey, D.L., Erickson, K.I., 2012. Increased body mass index is associated with a global and distributed decrease in white matter microstructural integrity. Psychosomatic Medicine 74(7):682–690.

[63] Birdsill, A.C., Oleson, S., Kaur, S., Pasha, E., Ireton, A., Tanaka, H., et al., 2017. Abdominal obesity and white matter microstructure in midlife. Human Brain Mapping 38(7):3337–3344.

[64] Ross, R., Neeland, I.J., Yamashita, S., Shai, I., Seidell, J., Magni, P., et al., 2020. Waist circumference as a vital sign in clinical practice: a Consensus Statement from the IAS and ICCR Working Group on Visceral Obesity. Nature Reviews. Endocrinology 16(3):177–189.

[65] Oka, R., Yagi, K., Sakurai, M., Nakamura, K., Nagasawa, S.Y., Miyamoto, S., et al., 2012. Impact of visceral adipose tissue and subcutaneous adipose tissue on insulin resistance in middle-aged Japanese. Journal of Atherosclerosis and Thrombosis 19(9):814–822.

[66] Van Dyken, P., Lacoste, B., 2018. Impact of metabolic syndrome on neuroinflammation and the blood-brain barrier. Frontiers in Neuroscience 12:930.

[67] Schulingkamp, R.J., Pagano, T.C., Hung, D., Raffa, R.B., 2000. Insulin receptors and insulin action in the brain: review and clinical implications. Neuroscience & Biobehavioral Reviews 24(8):855–872.

[68] Willette, A.A., Modanlo, N., Kapogiannis, D., Alzheimer's Disease Neuroimaging Initiative, 2015. Insulin resistance predicts medial temporal hypermetabolism in mild cognitive impairment conversion to Alzheimer disease. Diabetes 64(6):1933–1940.

[69] Iriondo, A., García-Sebastian, M., Arrospide, A., Arriba, M., Aurtenetxe, S., Barandiaran, M., et al., 2021. Plasma lipids are associated with white matter microstructural changes and axonal degeneration. Brain Imaging and Behavior 15(2):1043–1057.

[70] Williams, V.J., Leritz, E.C., Shepel, J., McGlinchey, R.E., Milberg, W.P., Rudolph, J.L., et al., 2013. Interindividual variation in serum cholesterol is associated with regional white matter tissue integrity in older adults. Human Brain Mapping 34(8):1826–1841.

[71] Bang, O.Y., Kim, J.W., Lee, J.H., Lee, M.A., Lee, P.H., Joo, I.S., et al., 2005. Association of the metabolic syndrome with intracranial atherosclerotic stroke. Neurology 65(2):296–298.

[72] Umene-Nakano, W., Yoshimura, R., Kakeda, S., Watanabe, K., Hayashi, K., Nishimura, J., et al., 2014. Abnormal white matter integrity in the corpus callosum among smokers: tract-based spatial statistics. PLoS One 9(2):e87890.

[73] Lin, F., Wu, G., Zhu, L., Lei, H., 2013. Heavy smokers show abnormal microstructural integrity in the anterior corpus callosum: a diffusion tensor imaging study with tract-based spatial statistics. Drug and Alcohol Dependence 129(1–2):82–87.

[74] Reaven, G., Tsao, P.S., 2003. Insulin resistance and compensatory hyperinsulinemia: the key player between cigarette smoking and cardiovascular disease? Journal of the American College of Cardiology 41(6):1044–1047.

[75] Sala, M., de Roos, A., van den Berg, A., Altmann-Schneider, I., Slagboom, P.E., Westendorp, R.G., et al., 2014. Microstructural brain tissue damage in metabolic syndrome. Diabetes Care 37(2):493–500.

[76] Portet, F., Brickman, A.M., Stern, Y., Scarmeas, N., Muraskin, J., Provenzano, F.A., et al., 2012. Metabolic syndrome and localization of white matter hyperintensities in the elderly population. Alzheimer's and Dementia 8(5 Suppl):S88–S95 e81.

[77] Dhollander, T., Raffelt, D., Connelly, A., 2017. Towards interpretation of 3-tissue constrained spherical deconvolution results in pathology. In: 25th International Society of Magnetic Resonance in Medicine, Honolulu, Hawaii.

